Dalton Transactions

Accepted Manuscript



This is an *Accepted Manuscript*, which has been through the Royal Society of Chemistry peer review process and has been accepted for publication.

Accepted Manuscripts are published online shortly after acceptance, before technical editing, formatting and proof reading. Using this free service, authors can make their results available to the community, in citable form, before we publish the edited article. We will replace this Accepted Manuscript with the edited and formatted Advance Article as soon as it is available.

You can find more information about *Accepted Manuscripts* in the **Information for Authors**.

Please note that technical editing may introduce minor changes to the text and/or graphics, which may alter content. The journal's standard <u>Terms & Conditions</u> and the <u>Ethical guidelines</u> still apply. In no event shall the Royal Society of Chemistry be held responsible for any errors or omissions in this *Accepted Manuscript* or any consequences arising from the use of any information it contains.



Incessant formation of chain-like mesoporous silica with superior binding capacity for mercury

S. Ravi, M. Selvaraj*

School of Chemical and Biomolecular Engineering

Pusan National University, Busan 609 735, Korea

* Corresponding Author

E-mail: chems@pnu.edu.

Tel.: +82 51 510 2397

Fax: +82 51 512 8563

Abstract: A novel incessant formation of chain like mesoporous silica (ICMS) has been easily materialized using mixed surfactants (Pluronic P123 and FC-4) as a structuring reagent in conjunction with thiol precursor (3–MPS) through one–pot synthetic method. A particular thiol concentration facilitated the interaction of micelle head groups to form long–chain micelles, where FC-4 enhanced further growth. The rapid interactions of micelles and the condensation of silicic acid and its oligomeric derivatives by coordinating 3–MPS through hydrogen bonding interactions leads to form ICMS. Characterization results of ICMS illustrated that they have ordered hexagonal pore geometry. The capability of ICMS for Hg²⁺ adsorption was extensively studied under different optimal parameters and the adsorption isothermal values clearly fits with Langmuir and Freundlich isothermal plots. This novel material exhibited an unprecedentedly high binding affinity toward even microgram levels of mercury ions in wastewater, compared to other thiol–based mesoporous silicas.

1. Introduction

The increasing anthropogenic contamination of ecosystem by mercury raises barriers to the initiative for environmental sustainability and this alarming level of mercury pollution should be dealt because it is considered to be toxic due to its volatility, persistence, bioaccumulation and health impacts on human beings. 1 Mercury pollution in the atmosphere is the consequence of industrial usages including burning coal to produce electricity, mining process, and using mercury in products such as fluorescent lights and dental fillings.² The mercury consumption is considered to be highly toxic because of its high affinity for thiol groups in proteins and enzymes, leading to unusual cell function and consequently many health problems in brain, kidney, immunity and central nervous system.³ Usually most of the toxic pollutant can be removed through the general techniques such as adsorption, ion exchange, precipitation and filtration.⁴ Among this adsorption technique is considered to be an economical and simplest way to remove mercury ions which has been carried out using various sorbents such as magnetic porous particles.⁵ mesoporous silicas⁶ and activated carbon⁷ etc. Interacting chemistry of sulfur with mercury suggesting the potential of mercaptan-derived compounds as valuable remediation materials for obtaining mercury-free water.8 Accordingly, the subject of sulfur-mediated mercury remediation has grown into a dynamic field of contemporary research, as evidenced by the ample number of reports; particularly sulfur functionalized; mesoporous silicas, ^{6a,6b} mesoporous carbon, magnetic porous particles and organic resins the mercury content of wastewater with a concentration level <1 µg/L remains challenging by contemporary purification techniques.

Owing to the peculiar physical properties of structurally modified mesoporous silica materials,

including pore channel networks, particle size & shape, and large internal surface areas, have attracted worldwide interest in applications such as heavy-metal adsorption, 10 controlled drug release, 11 chemical sensors 12 and catalysis 13. When it comes to metal adsorption, it has long been demonstrated that the structural and textural parameters of silica material directly influences their adsorptive abilities. 14 The synthesis of fiber-like hexagonal mesoporous silica in the presence of organic functional materials through a surfactant self-assembly are thus of particular importance in the above context and it has been extensively investigated in the current decade. 15 The tailoring and control of mesoporous silica morphology using organic precursors has seen continuous investigation in materials synthesis, a typical example being the case of helical mesoporous silica. 16 The molecular arrangement of surfactant micelle segments using organic precursors has been previously reported, with particular focus on organic groups, which allows them a simple and intuitive insight into the self-assembly phenomenon, ^{17,18} thus, direct one-pot immobilization methods have been frequently reported in order to improve the physicochemical properties of organo-functionalized hybrid mesoporous silica materials. As far we know, no synthetic routes have been reported in the literature for modifying the pore surfaces of fluorocarbon co-surfactant-mediated synthesis of mesoporous silica by direct insertion of organosilanes. An assembled layer of fluorocarbon surfactant FC-4¹⁹ with nonionic surfactant favors the particle size and morphology control. Moreover, a unique structure of mesoporous materials is achieved by judiciously choosing different ratios of FC-4, Pluronic P123 surfactant, and (3-Mercaptopropyl)trimethoxysilane (3-MPS). Numerous reports have been published on thiol functionalized mesoporous silica materials for the adsorption of Hg2+ ions which is elaborately discussed in the peer review article²⁰ and among the thiol functionalized silicas most of the materials exhibits low saturation binding towards Hg^{2+} ions due to the poor structural

properties and there are some of reports describing the potential use of mercapto functionalized silica materials to adsorb mercury ions.²¹

Herein, we report a novel one-step pathway for the preparation of incessant chain like mesoporous silica materials (ICMS) with continuous pore channels and high concentration of sulfur precursor bonded on the surface of pore walls. Finally, the as-prepared ICMS materials were investigated for their efficacies towards the removal of mercury metal ions. To the best of our knowledge, this is the first attempt towards the use of newly designed ICMS materials for mercury adsorption studies.

2. Experimental Section

2.1. Material synthesis

The synthesis of incessant chain like mesoporous materials by the solvothermal method employs the following chemicals Pluronic P123/FC–4/TEOS/HCl/H₂O²² and 3–MPS. Typically Pluronic P123 was dissolved in aqueous HCl solution with magnetic stirring until the clear solution was obtained. Subsequently, fluorocarbon surfactant was added with magnetic stirring and stirred for further 3 h. This is followed by the addition of TEOS (1–X mol) to the solution; and the pH (1.6–1.8) was maintained up to the prehydrolysis time for 3–4 h, successively thiol precursor 3–MPS (X=0.1, 0.2, and 0.3 mol) was added to the consecutive reaction mixture. The resulting mixture was stirred for further 24 h at 30°C, and then transferred to Teflon–lined stainless steel autoclave and heated to 100°C for 24–36 h. The obtained materials were filtered and washed, using distilled water followed by ethanol, and dried in vacuum at 60 °C for 6 h and then ehanolic

solution were taken to remove the surfactant from the as–synthesized materials. The as–synthesized material were dispersed in ethanol:HCl mixture (99:1) and refluxed for 24 h. The refluxed materials were filtered and washed using hot ethanol and the above processes were repeated for three times and then the obtained material was evacuated for 6 h to remove the traces of solvents. Sulfur groups are likely to be distributed homogeneously by this method, which can be further confirmed by characterization. Thus, the preparation of long–channeled thiol–functionalized ICMS was achieved.

2.2. Characterization

Field emission Scanning electron microscope (SEM) images measurement were recorded on a JEOL JSM–6700F instrument. Transmission electron microscope (TEM) images measurements were recorded on a JEOL 2010 electron microscope operating at 200 kV. The powder samples were dispersed in ethanol, then deposited and dried on a perforated Cu grid. Images were recorded at magnifications 150,000× and 200,000×. Small angle X–ray scattering (SAXS) was performed at the Pohang Accelerator Laboratory (PAL) (POSTECH, South Korea) with Co–K α radiation (λ = 1.608 Å) in the energy range 4–16 keV (energy resolution: Δ E/E = 5 × 10⁻⁴; photon flux: 10¹⁰–10¹¹ ph./s, Beam size: <1 mm²) over the scan range 0.4 nm⁻¹ < q < 5.0 nm⁻¹. Nitrogen adsorption and desorption isotherms were measured using an ASAP 2020 surface—area and pore—size analyzer. Prior to the measurement, the samples were dehydrated at 90 °C for 5 h. The BET (Brunauer–Emmett–Teller) method was used to calculate the specific surface area. The pore size distribution was calculated from the analysis of the isotherm desorption branch by the BJH (Barret–Joyner–Halenda) method coupled with the apparatus software. Elemental analyses were measured on vario MICRO CHNS analysis technic. The infrared spectra were recorded on

a Nicolet 6700 FT–IR spectrometer. Solid state 29 Si CP/MAS NMR measurements were carried out on a Bruker ADVANCE II⁺ 400MHZ NMR system. Magic angle spinning was performed at 6 kHz spinning rate and the contact time was fixed at 2ms in all the experiments. XPS analysis was performed using an X–ray photoelectron spectrometer (VG, ESCALAB 250) with monochromatic Al K α radiation (hv = 1486.6 eV).

Adsorption studies

The adsorption behaviors of mercury onto ICMS were investigated by batch adsorption experiments on a rotary shaker at 200 rpm using 50 mL glass vials. In a typical experiment, 20 mg of ICMS–30 was added to 20 mL mercury solution with different initial concentrations (10, 50, 75, 100 and 125 mg L^{-1}). The reaction temperature was kept constant at 25 ± 0.2 °C (room temperature), and the solution pH was not adjusted. From the experiments the equilibrium constant (q_e) were determined by,

$$q_e = (c_i - c_e) \times (v/m)$$

Where c_i (mg L^{-1}) is the initial concentration, c_e (mg L^{-1}) is the equilibrium concentration, v (L) denotes the volume of the mercury solution, and m (g) is the mass of the adsorbent. The prologue investigations were carried out in batches in different conditions of pH, time and initial concentrations of mercury ions to check the propensity of adsorption process. The distribution coefficient (K_d) measurements were carried out for ICMS materials using 8.0–10.0 ppm of Hg²⁺ solutions, using the following equation

$$K_d = [(c_i - c_f)/c_f] \times (v/m)$$

Where c_i (mg L^{-1}) is the initial concentration, c_f (mg L^{-1}) is the final concentration, v (ml) is the volume of the mercury solution, and m (g) is the mass of the adsorbent. After 24 h, samples were removed, filtered through a 0.2- μ m filter, and analyzed for mercury content. The Hg^{2+} quantity was determined using Direct Mercury Analyzer (DMA-80, Milestone).

3. Results and discussion

3.1. Influence of (3-mercaptopropyl)trimethoxysilane on mesoporous silica

ICMS was synthesized by the co-condensation of Tetraethylorthosilicate (TEOS) and 3-MPS using a surfactant mixture comprising Pluronic P123 and FC-4. The amount of 3-MPS was varied from 10 to 30 mol% in order to investigate mesopore morphological changes from rod-like to continuous chain like channel networks. The direct one-pot method was applied to infuse the thiol precursor into the template-assembled reaction mixture. The synthesized ICMS material obtained from this process was found to have an ordered hexagonal pore structure; the resultant incessant chain like formation of the final product was found to be dependent on the concentration of 3-MPS.

In the absence of 3–MPS, the synthesized mesoporous material possessed a primarily rod–like morphology; however, the addition of a small amount of 3–MPS (10%) by the direct co-condensation method resulted in the formation of chain like mesostructured materials. The FE–SEM and TEM images displayed in figure (1) depict the morphologies of IBN–4²² and ICMS, which comprise a hexagonal packing geometry. The development of ICMS continuous pore structure occurred by the formation of covalent bonds between Si and O atoms, is enhanced by the presence of thiol compounds.

SAXS measurements depicting the lattice pattern for thiol-functionalized mesoporous IBN-4 with 0, 10, 20, and 30 mol% of 3-MPS are designated in figure (2) such as a, b, c, and d respectively. The lattice pattern of sample 'a' exhibited three well-resolved characteristic diffraction peaks that could be indexed to (100), (110), and (200) reflections, which represent the highly ordered mesoporous IBN-4 with a 2D hexagonal symmetry (p6m). Moreover, reduction in peak intensities from a-d with increasing thiol concentration, suggesting the organosilane have been successfully functionalized into the ICMS materials. In addition the d-spacing value for IBN-4 is 6.9 nm is tending to increase upon increasing the 3-MPS loading as shown in table (1). Nitrogen physisorption experiments were performed to study the changes in the textural properties of the functionalized mesoporous materials. The nitrogen adsorption isothermal plots of all the thiol functionalized materials showed type IV isotherms is displayed in figure (3a). 23,24 These observations were associated with the capillary condensation in hexagonal cylindrical mesopores; at relative pressures of p/p_0 0.4 – 0.8, large porous mesostructures with specific BET surface areas of 486, 355, and 302 m²/g were obtained for ICMS materials with 10, 20, and 30 mol% thiol loading respectively. Notably, a decrease in the surface area value was directly correlated with increase in the thiol content of mesoporous materials. IBN-4 possess type IV isotherm with H1 hysteresis loop (Figure S1) but ICMS-10, ICMS-20 and ICMS-30 exhibit typical H2 hysteresis loops due to the "ink-bottle" pore formation. Introduction of thiol precursors into the mesoporous materials shapes different pore sizes but despite the high loading of thiol groups, ICMS-30 possesses uniform pore size distribution as shown in figure (3b). ICMS-30 differs in the desorption branch where the convergence of adsorption and desorption branches is downshifted to $P/P_0 \sim 0.41$, in comparison with ~ 0.45 for ICMS-10. Moreover, the sharp desorption lines and delayed convergence of the two branches often happens to pores

possessing a bottleneck–type structure, in which the entrance is smaller than the internal pore.²⁴ The observed hysteresis loops show that they belongs to different types of pore structures when high concentrations of 3–MPS are introduced, i.e. the hysteresis loop is shifted from cylindrical shape²² to ink–bottle type. The capillary condensation shifted gradually to a lower vapor pressure in the X–axis with an increase in the 3–MPS content which could be attributed to decreasing pore diameter values. The obtaining H₂ hysteresis loop and the progressive variation of pore diameter and pore volume values from ICMS–10 to ICMS–30 in table (1) are suggesting the ink bottle pore formation due to the amount of thiol binding on the pore entrances of ICMS.

The presence of organic groups in the ICMS materials was confirmed by the FT–IR spectroscopic analysis. The FT–IR spectra of ICMS are displayed in figure (4). The propyl groups attached to the silicon framework were confirmed by the –CH₂– stretching bands present in the region 2930 cm⁻¹, corroborating the attachment of organic moieties onto the silica surface; the peak intensities were found to increase with an increase in the molar percentage loading of 3–MPS (Figure S2). Similarly the band at 1446 cm⁻¹ was assigned to the –CH₂– symmetric bending mode vibration. Moreover, a large broad band between 3500 and 3200 cm⁻¹ was observed, which was attributed to the O–H stretching mode of silanol groups. The absorption bands at 1094 and 800 cm⁻¹ were assigned to Si–O–Si and Si–O stretching vibrations, respectively; characteristic bands at 952 cm⁻¹ were assigned to Si–OH stretching vibrations.

The extent of thiol moiety incorporated into the mesoporous silica was further identified through ²⁹Si–CP/MAS NMR spectra (Figure 5). The spectrum of ICMS shown three peaks at the range of –110, –100, and –92 ppm are attributed to silicon in the siloxane binding environment without hydroxyl group [(SiO)₄Si], isolated silanol group [(SiO)₃Si–OH] and to geminal silanol groups

[SiO]₂Si–(OH)₂] of the silica support which are denoted as Q^4 , Q^3 and Q^2 respectively.²⁵ In addition to these peaks, two additional peaks can be observed at the range of –57 and –66 ppm, which corresponds to two different environments for the siloxane groups i.e., 3–MPS functionalized layers and these are represented as T^2 and T^3 respectively. Distinguishable peaks at –111, –100 were recorded for the silica support and an increase in Q^3 was observed along with reduction of Q^4 peak with simultaneous increase in T^3 , with increasing thiol precursor concentration in ICMS materials. The quantitative determinations of sulphur in the ICMS materials were done by elemental analysis and the corresponding values are given in table (1) and weight percentages of rest of elements were also measured and summarized in table (S1).

Further corroboration for the existence of thiol group in ICMS-30 was provided through XPS analysis (Figure 6). In this case a sole characteristic thiol (-SH) sulphur 2p binding energy peak at 163.3 eV was observed.²⁶ Moreover, no detectable oxidized species like -SO₃⁻ (169 eV) or -SS- (168.8 eV) were present. The obtained S2p peak region confirming the presence of fluorocarbon does not affect the nature of thiol groups.

Expansion of chain length by increasing concentration of thiol groups during synthesis directly affected the lateral dimensions of the resultant nanostructures; as noted by TEM images in figure (7a₁–c₁). FE–SEM images in the figure (7a–c) depict that at higher concentration of thiol groups, the cluster type ICMS materials were organized due to the particle interaction. It is worth noting that such structural modification was minimal in a prior report that described in the synthesis of hexagonal helical–type mesoporous silica.¹⁶ An optimized 3–MPS amount of 30 mol% provided ideal change in the particle length, uniformity, and pore density of the ICMS materials. At lower thiol concentration the obtained ICMS particle sizes were ranging about 300–500 nm but at

higher concentration i.e. >10% of 3–MPS, the mesopore particles length found to increase about greater than 1μm range. These structural alignments depend on the thiol substrate, guiding the long–channeled mesoporous silica system and it's made realistic changes on mesoporous structuring, where the alignment of mesoporous channels and pore volume was affected by the use of high aspect ratio of thiol precursor. The SAXS patterns revealed a reduction in lattice pattern peak intensity with a higher concentration of thiol groups and the TEM images of ICMS–30 shown vague pore channels are suggesting that infusion of >30 mol% of 3–MPS to the mesoporous silica can significantly disturb the pore channels and hexagonal morphologies of ICMS as shown in figure (S3).

This change in morphology is caused by several interactions viz; electrostatic forces, hydrogen bonding, and hydrophobic interaction between the thiol precursor and surfactant molecules. Insertion of thiol precursor into the mesoporous material is achieved by its attraction to the hydrophobic terminal of the Pluronic P123 polymer surfactant¹⁸ and this attractive force attributed to organosilane which promotes the extension of FC–4 from the micelles, forming a linear aggregation with neighboring particles through silicic bond formation. It has been hypothesized that the strong interactions of micelle head groups with silicic acid and its oligomers via hydrogen bonding are key features in the formation of ICMS. Cylindrical type micelles are flexible to change their morphology by the addition of organo silanes.^{16,27} We noted that an increase in 3–MPS tend to increase the hydrophobicity of ICMS to a certain extent, eventually resulting in a reduction in ICMS particle dimensions, which can enhance the surface chemistry of thiol group. Possibly, increasing surface chemistry of sulfur atoms can improve the adsorption efficiency of ICMS towards Hg²⁺ ions.

3.2. Adsorption studies

3.2.1. Adsorption isotherm

The equilibrium adsorption isotherm is one measure to understand the mechanism of adsorption systems. In order to conduct adsorption studies, a mixture of the synthesized ICMS materials with aqueous solutions containing known amounts of Hg^{2+} was prepared. The mixture was stirred until the equilibrium was reached. The adsorption isotherm of Hg^{2+} at room temperature is shown in figure (8a).

There is increase in the equilibrium adsorption capacity with increasing initial concentration of Hg²⁺. The Langmuir and Freundlich isothermal datas are widely used to investigate the isothermal data. These isotherms not only explain adsorption capacity but also give insight about surface properties and adsorbent/adsorbate affinity constants. The Langmuir isotherm model assumes that adsorption takes place at specific homogeneous sites within the adsorbent by monolayer adsorption without any interaction between adsorbed molecules. The parameters of Langmuir isotherm are established by the following relation: ²⁸

$$\frac{c_e}{q_e} = \frac{1}{bq_m} + \frac{c_e}{q_m}$$

Where c_e is the equilibrium concentration of adsorbate entities in the solution (mg L^{-1}) q_e defines the amount of adsorbate entities adsorbed on the unit amount of the adsorbent at equilibrium (mg g^{-1}), q_m represents the maximum adsorption capacity of adsorbent (mg g^{-1}), and b is defined as the affinity of binding sites or the Langmuir constant (L mg⁻¹). The Hg²⁺ adsorption isotherm of ICMS-30 exhibits typical Langmuir behavior similarly like other mercapto functionalized

mesoporous materials²⁹, suggesting monolayer adsorption on independent binding sites.

Besides, the Freundlich model describes the adsorption of a reversible heterogeneous surface since it is not restricted to the monolayer adsorption capacity which is given by,

$$\ln q_e = \ln K + \frac{1}{n} \ln c_e$$

Where K and i/n are constants designated for indicative of adsorption capacity and intensity of adsorption respectively. By using adsorption kinetics datas, the Langmuir and Freundlich isotherm model has been drawn which were shown in figure (8b) and figure (8c) respectively. From Langmuir isotherm model and Freundlich isotherm model, the maximum binding capacity noted for the ICMS-30 is that of 401 mg/g and the calculated Langmuir constant (b), adsorption intensity (1/n) has been summarized in the table (2). From the experimentally determined q_m value and assuming a 1:1 S/Hg stoichiometry in the complex, one can easily calculate the existence of chemically active sulphur groups onto the pore network is 2.0 mmol/g of ICMS-30. For Langmuir adsorption isotherm the calculated correlation coefficient factor (R²) is 0.9957 and for Freundlich model, the calculated R² is 0.9911, higher values of correlation coefficients indicates that the Langmuir model fits well the isotherm compared to the Freundlich model.

Effect of pH, time and initial concentration of mercury ions

The adsorption capacity of an adsorbent for metal ions not only depends on the chemical and physical properties of the adsorbent and the target metal ions, including the conditions of sample matrix such as the pH and hydrolysis capacity of the metal ions. Effect of pH on Hg²⁺ adsorption percentages of ICMS–30 material with 10 ppm of Hg²⁺ solution was determined and their corresponding mercury–removal efficiencies are shown in figure (9a). An examination of ICMS

treated over long and short sorption times in a wide range of pH conditions revealed optimum levels of adsorption obtained at pH 5. The abundance of negatively charged surface sites decreases and the number of positively charged sites rises due to protonation effect nearing to lower pH(<3) conditions, and hence due to the decreasing electrostatic repulsion the Hg²⁺ adsorption percentage is rises from the lower pH conditions to basic condition.^{30,31} Simultaneously due to instability of silica at higher pH(>8) the Hg²⁺ adsorption percentages decreases compare to the optimum level of adsorption. However, the variation of Hg²⁺ adsorption percentage by ICMS–30 is significant at lower initial concentration of mercury ions with wide pH conditions to examine the minute changes in the adsorption process.

Efforts toward the development of mesostructured silica for mercury adsorption have been mostly concerned with the incorporation of thiol groups, because sulfur possesses a strong affinity for mercury according to the principle of hard and soft Lewis acids and bases.⁸ All the ICMS samples were analyzed for mercury adsorption studies, in which ICMS–30 showed superior results compared to the remaining two materials which is shown in figure (9b). After adsorption treatment, all ICMS materials showed quite similar results when the Hg²⁺ initial concentration is ≤100 ppm; that is, approximately ~99% of mercury were removed from the initial concentrations. Interestingly, only the ICMS–30 remains the ~98% removal efficiency, it been maintaining up to 250ppm initial concentration of Hg²⁺ solution. This significant mercury removal efficiency of ICMS–30 was noted with different time interval and the observed results showed that within 5 to 10 minutes the adsorption capacity reached to 98%, and it took further 12 to 24 hours to reach maximum percentage, which is shown in figure (9c).

3.2.2. Distribution coefficient

The adsorption efficiency of ICMS materials was also determined from the distribution coefficient (K_d) value. ICMS materials with different concentrations of thiol groups were examined to investigate the mercury-adsorption capabilities in wastewater. Generally, sorbents with K_d values greater than 10⁴ are considered to be ideal. In some cases greater affinity of thiol groups towards Hg^{2+} results extremely low residual mercury in the aqueous solution after the adsorption process enables higher distribution coefficient (K_d) values in the range of ~10⁸ ml/g. The ICMS materials synthesized in this work showed significant K_d values i.e. the order of $>10^5$ and the obtained K_d values are summarized in table (3). In this study, the calculated K_d value for ICMS-30 with 10 ppm initial concentration of Hg²⁺ solution is in the order of 10⁷, which is analogous to the reported K_d value of SAMMS;^{21e} however, ICMS exhibit slower adsorption rate as that of SAMMS (self-assembled monolayer on mesoporous silicas). However the moderate hydrophobicity of ICMS-30 due to the higher concentration of alkyl chain and the bottle neck pore nature reduces the diffusivity of mercury ions towards aqueous medium, resulting better activity in the adsorption process. The uniform pore sizes of ICMS-30 due to bottle neck formation, is also a reason for its higher capacity and equilibrium constant towards mercury adsorption.

More porous particles exhibit improved sorption activities in diffusion–limited systems;¹⁷ the extended length of ICMS–30 has a potentially greater capability to remove the hazardous mercury from wastewater. Adsorption processes are not only dependent on surface area and pore size distribution; an additional factor observed here is that the reduction in the particle diameter enhances the surface thiol–binding chemistry with Hg²⁺ and results in a more efficient mercury sorption.

3.2.3. Adsorbent regeneration:

Recycling and regeneration of adsorbent has significant part in the sorption studies of practical applications. Typically, 0.1 g of mercury–loaded adsorbent(ICMS–30) was treated with 50 mL of acidified thiourea (3M HCl+2% thiourea solution) and stirred for 6 h at room temperature and then the regenerated adsorbent sample was thoroughly washed with ethanol, water, and dried at 60 °C for 12 h. The first regenerated adsorbent was treated for mercury adsorption, shown >99% mercury removal in the 2nd cycle. Then the materials were regenerated by using the same procedure and used for repetitive cycles. Interestingly 98%, 95% were conceded for third and fourth cycles. The removal efficiency is slightly reduced in the subsequent cycles; however, it is still above 89% in the sixth cycle (Figure 10). This indicated that the chemisorption activity of the ICMS–30 samples was still high even after 5 regenerations.

4. Conclusion

We have described the facile synthesis of ICMS material for the removal of mercury ions from the aqueous medium. The reagents used in the preparation of ICMS (3–MPS and FC–4) had a significant role in determining the chain like shape and ink bottle pore formation. This proposed method represents a relevant and direct approach to design a novel chain like, continuous—channeled mesoporous silica nanoparticles for the removal of environmentally toxic pollutants. The significance of this new ICMS material is that the synthesis is simple, showed excellent mercury adsorption, exhibiting higher binding capacities as compared to previously described silica–based materials. We suggest that the reduction in particle diameter and chain like transformation of ICMS are considered for their higher activities on Hg²⁺ uptake.

Acknowledgements

This research work was supported by BK21 PLUS Centre for Advanced Chemical Technology funded by Korean government (21A20131800002).

References

- A. Renzoni, F. Zino and E. Franchi, *Environ. Res.*, 1998, 77, 68–72. b) M. Park, S. Seo, I.
 S. Lee and J. H. Jung, *Chem. Commun.*, 2010, 46, 4478–4480. c) X. L. Zhang, Y. Xiao and X. H. Qian, *Angew. Chem. Int. Ed.*, 2008, 47, 8025–8029. d) M. Greger, Y. Wang, and C. Neuschutz, *Environ. Poll.*, 2005, 134, 201–208.
- a) R. J. von Burg, *Appl. Toxicol.*, 1995, 15, 483–493. b) H. H. Harris, I. J. Pickering and G. N. George, *Science*, 2003, 301, 1203.
- C. S. Eckley, M. T. Parsons, R. Mintz, M. Lapalme, M. Mazur, R. Tordon, R. Elleman, J. A. Graydon, P. Blanchard and V. S. Louis, *Environ. Sci. Technol.*, 2013, 47, 10339–10348.
- 4. a) W. Gao, M. Majumder, L. B. Alemany, T. N. Narayanan, M. A. Ibarra, B. K. Pradhan, and P. M. Ajayan, *ACS Appl. Mater. Interfaces*, 2011, **3**, 1821–1826. b) F. D. Natalea, A. Ertoa, A. Lanciaa, D. Musmarra and *J. Hazard. Mater.*, 2011, **192**, 1842–1850. C) S. Chiarle, M. Ratto, M. Rovatti and *Water research*, 2000, **34**, 2971–2978.
- a) A. Sinha and N. R. Jana, *Chem. Commun.*, 2012, 48, 9272–9274. b) F. He, W. Wang, J. Moon, J. Howe, E. M. Pierce and L. Liang, *ACS Appl. Mater. Interfaces*, 2012, 4, 4373–4379. c) X. Chen, K. F. Lam, Q. Zhang, B. Pan, M. Arruebo and K. L. Yeung, *J. Phys.*

- Chem. C, 2009, **113**, 9804–9813. (d) J. Liu and X. Du, J. Mater. Chem., 2011, **21**, 6981–6987. e) K. Cheng, Y. M. Zhou, Z.Y. Sun, H. B. Hu, H. Zhong, X. K. Konga and Q. W. Chen, Dalton Trans., 2012, **41**, 5854–5861.
- a) H. Y. Wu, C. H. Liao, Y. C. Pan, C. L. Yeh and H. M. Kao, *Microporous Mesoporous Mater*. 2009, 119, 109–116.
 b) E. D. Canck, L. Lapeire, J. D. Clercq, F. Verpoort and P. V. D. Voort, *Langmuir*, 2010, 26, 10076–10083.
 c) L. Bai, H. Hu, W. Fu, J. Wan, X. Cheng, L. Zhuge, L. Xiong and Q. Chen, *J. Hazard. Mater.*, 2011,195, 261–275.
- 7. a) H.□C. Hsi, M.□J. Rood, M. Rostam–Abadi, S. Chen and R. Chang, *Environ. Sci. Technol.*, 2001, **35**, 2785–2791. b) W. Liu, R.□D. Vidic and T.□D. Brown, *Environ. Sci. Technol.*, 2000, **34**, 483–488.
- 8. R. G. Pearson, *Science*, 1966, **151**, 172–177.
- 9. Y. Shin, G. E.Fryxell, W. Um, K. Parker, S. V. Mattigod and R. Skaggs, *Adv. Funct. Mater.*, 2007, **17**, 2897–2901.
- a) A. Bibby and L. mercier, *Chem. Mater.*, 2002, 14, 1591–1597. b) A. M. Liu, K. Hidajat, S. Kawi and D. Y. Zhao, *Chem. Commun.*, 2000, 1145–1146. c) J. Aguado, J. M. Arsuaga and A. Arencibia, *Ind. Eng. Chem. Res.*, 2005, 44, 3665–3671. d) J. Liuab and X. Du, *J. Mater. Chem.*, 2011, 21, 6981–6987. e) S. A. Idrisa, C. M. Davidsona, C. McManamonb and M. A. Morrisb, *J. Hazard. Mater.*, 2011, 185, 898–904.
- N. Mal, M. Fujiwara, Y. Tanaka and *Nature*, 2003, **421**, 350–353. b) Y. Chen, H. Chen,
 M. Ma, F. Chen, L. Guo, L. Zhanga and J. Shi, *J. Mater. Chem.*, 2011, **21**, 5290–5298. c)
 P. Yang, S. Gai and J. Lin, *Chem. Soc. Rev.*, 2012, **41**, 3679–3698.

- 12., P. Van Der Voort, C. Vercaemst,, D. Schaubroeck and F. Verpoort, *Phys. Chem. Chem. Phys.*, 2008, **10**, 347–360.
- a) I. K. Mbaraka, D. R. Radu, V. S.-Y. Lin and B. H. Shanks, *Journal of Catalysis*, 2003,
 219, 329–336. b) C. Jiang, K. Hara and A. Fukuoka, *Angew. Chem. Int. Ed.*, 2013, 52,
 6265 –6268. c) E. Gross, J. Liu, S. Alayoglu, M. A. Marcus, S.C. Fakra, F. D.Toste and G. A. Somorjai, *J. Am. Chem. Soc.*, 2013, 135, 3881–3886. d) C. M. A. Parlett, K. Wilson and A. F. Lee, *Chem. Soc. Rev.*, 2013, 42, 3876–3893.
- 14. C. Delacotea, F. O. M. Gaslainc, B. Lebeauc and A. Walcarius, *Talanta*, 2009, **79**, 877–886.
- F. Rambaud, K. Valle, S. Thibaud, B. Julian–Lopez and C. Sanchez, *Adv. Funct. Mater.*,
 2009, 19, 2896–2905.
- a) L. Zhang, S. Qiao, Y. Jin, L. Cheng, Z. Yan and G. Q. Lu, *Adv. Funct. Mater.*, 2008,
 3834–3842. b) W.–C. Huang, N.–C. Lai, L.–L. Chang and C.–M. Yang, *Microporous Mesoporous Mater.* 2012, 151, 411–417.
- 17. a) C. Gao, Y. Sakamoto, O. Terasaki, K. Sakamoto and S. Che, *J. Mater. Chem.*, 2007,
 17, 3591–3602. b) S. Che, A. E. Garcia–Bennett, T. Yokoi, K. Sakamoto, H. Kunieda, O. Terasaki and T. Tatsumi, *Nature*, 2003, 2, 801–805.
- 18. S. Huh, J. W. Wiench, J.Yoo, M. Pruski and V. S. Y. Lin, *Chem. Mater.*, 2003, **15**, 4247–4256.
- 19. a) R. Xing, H.-J. Lehmler, B. L. Knutson and S. E. Rankin, *Langmuir*, 2009, 25, 6486-

- 6492. b) B. Tan, H.–J. Lehmler, S. M. Vyas, B. L. Knutson and S. E. Rankin, *Chem. Mater.*, 2005, **17**, 916–925. c) D. Li, Y. Han, J. Song, L. Zhao, X. Xu, Y. Di and F. S. xiao, *chem. Eur. J.*, 2004, **10**, 5911–5922.
- 20. A. Walcarius and L. Mercier, *J. Mater. Chem.*, 2010, **20**, 4478–4511.
- 21. a) L. Mercier and T. J. Pinnavaia, *Environ. Sci. Technol.*, 1998, 32, 2749–2754. b) X. Feng, G. E. Fryxell, L.–Q. Wang, A. Y. Kim, J. Liu and K. M. Kemner, *Science*, 1997, 276, 923–926. c) Y. Mori and T.□J. Pinnavaia, *Chem. Mater.*, 2001, 13, 2173–2178. d) C.□C. Chen, E.□J. McKimmy, T.□J. Pinnavaia and K.□F. Hayes, *Environ. Sci. Technol.*, 2004, 38, 4758–4762. e) J. Liu, X. Feng, G. E. Fryxell, L. Wang, A. Y. Kim and M. Gong, *Adv. Mater.*, 1998, 10, 161–165.
- 22. Y. Han and J. Y. Ying, *Angew. Chem. int. Ed.*, 2005, 44, 288–292.
- 23. K. Sing, D. Everett, R. Haul, L. Moscou, R. Pierotti, J. Rouquerol and T. Siemieniewska, *Pure Appl. Chem.*, 1985, **57**, 603–619.
- 24. L. Sarkisov and P. Monson, *Langmuir*, 2001, **17**, 7600–7604.
- 25. P. T. Tanev and T. J. Pinnavaia, *Chem. Mater.*, 1996, **8**, 2068–2079.
- a) N. Shevchenko, V. Zaitsev and A. Walcarius, *Environ. Sci. Technol.*, 2008, 42, 6922–6928.
 b) A. Walcarius and V. Ganesan, *Langmuir*, 2006, 22, 469–477.
- S. Yang, L. Zhao, C. Yu, X. Zhou, J. Tang, P. Yuan, D. Chen and D. Zhao, *J. Am. Chem. Soc.*, 2006, 128, 10460–10466.
- 28. I. Langmuir, J. Am. Chem. Soc., 1918, 40, 1361–1403.

- 29. S. Aytasa, M. Yurtlua and R. Donatb, J. Hazard. Mater., 2009, 172, 667-674.
- 30. F. Raji and M. Pakizeh, Applied Surface Science, 2013, 282, 415–424.
- 31. A. Sari and M. Tuzen, J. Hazard. Mater., 2009, 171, 500-507.

Figures

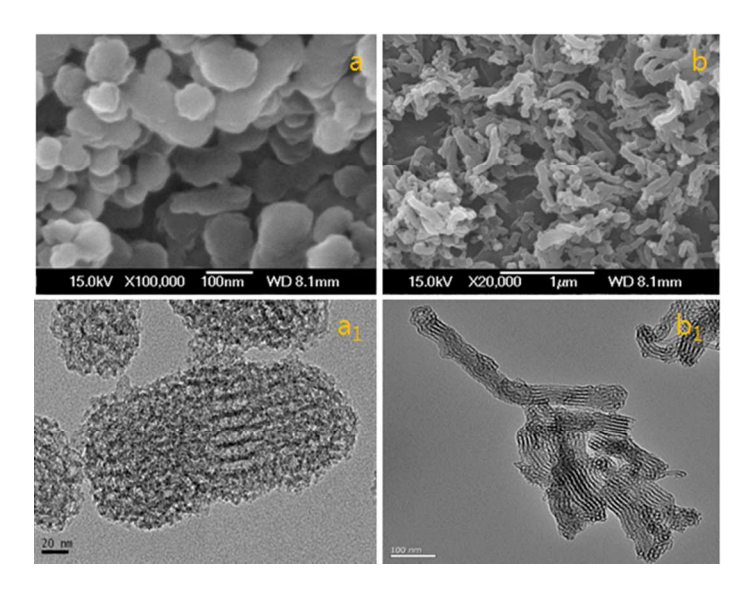


Figure 1. FE–SEM images for IBN–4 and ICMS materials are 'a' and 'b' respectively. TEM images for IBN–4 and ICMS materials are 'a₁' and 'b₁' respectively.

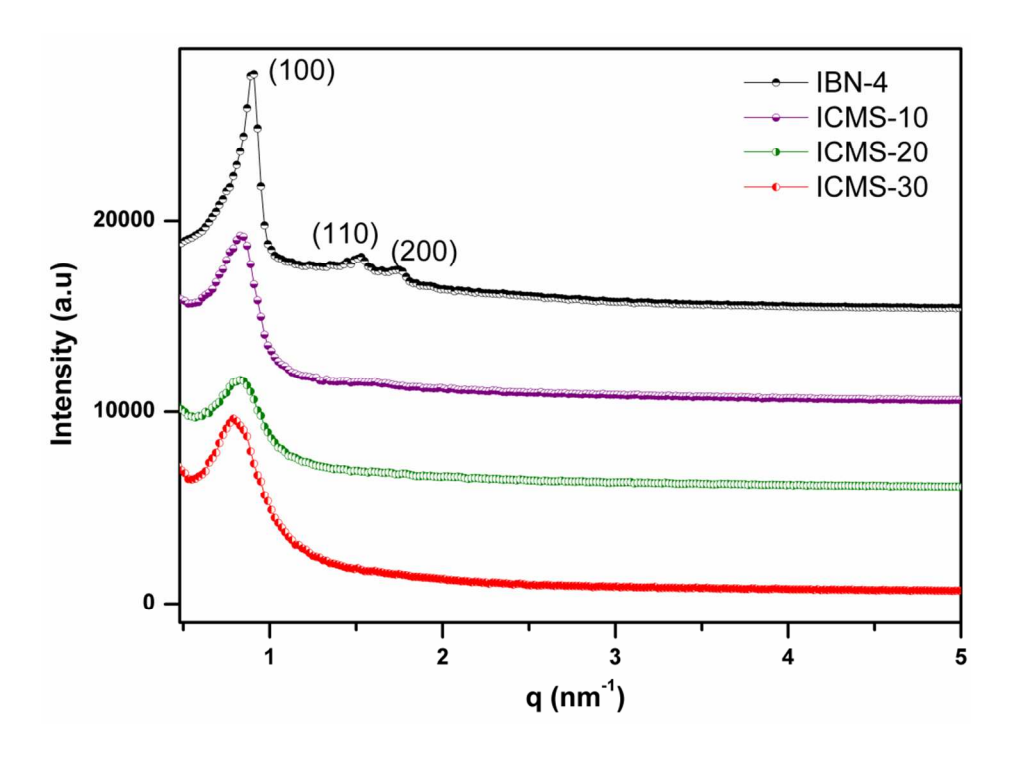


Figure 2. SAXS patterns of IBN–4 and ICMS materials; IBN–4 (a), ICMS–10 (b), ICMS–20 (c), and ICMS–30 (d). (3–MPS mole percentages, 10 %, 20 % and 30 % were used in the preparation of ICMS–10, ICMS–20 and ICMS–30, respectively).

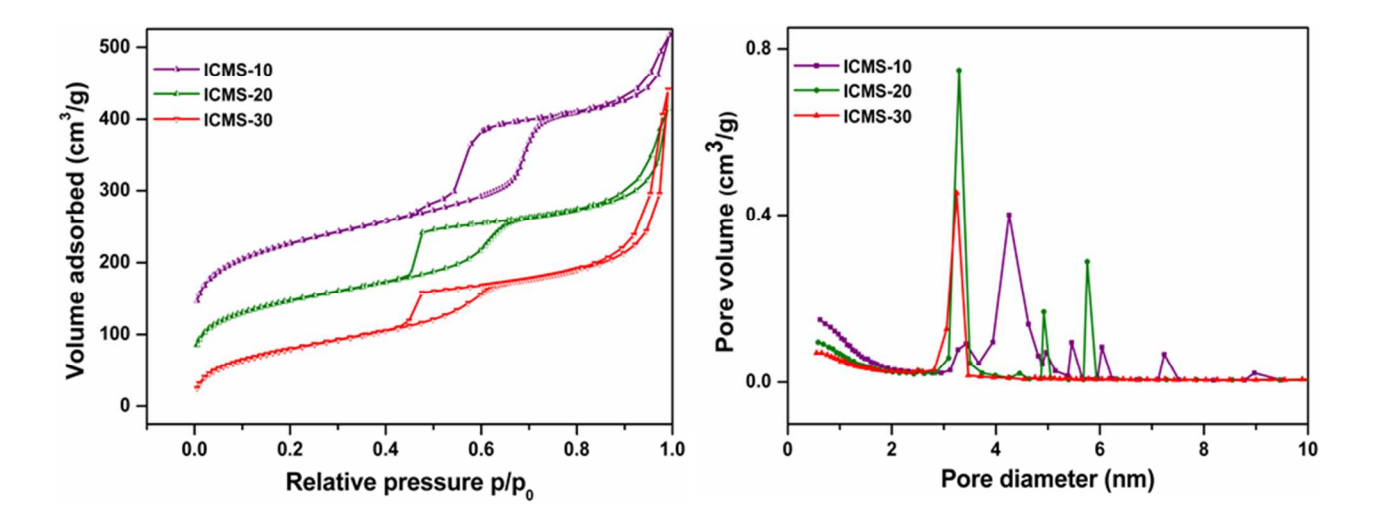


Figure 3. a) N₂ adsorption –desorption isotherm of ICMS materials, b) BJH Pore size distribution curve of ICMS material.

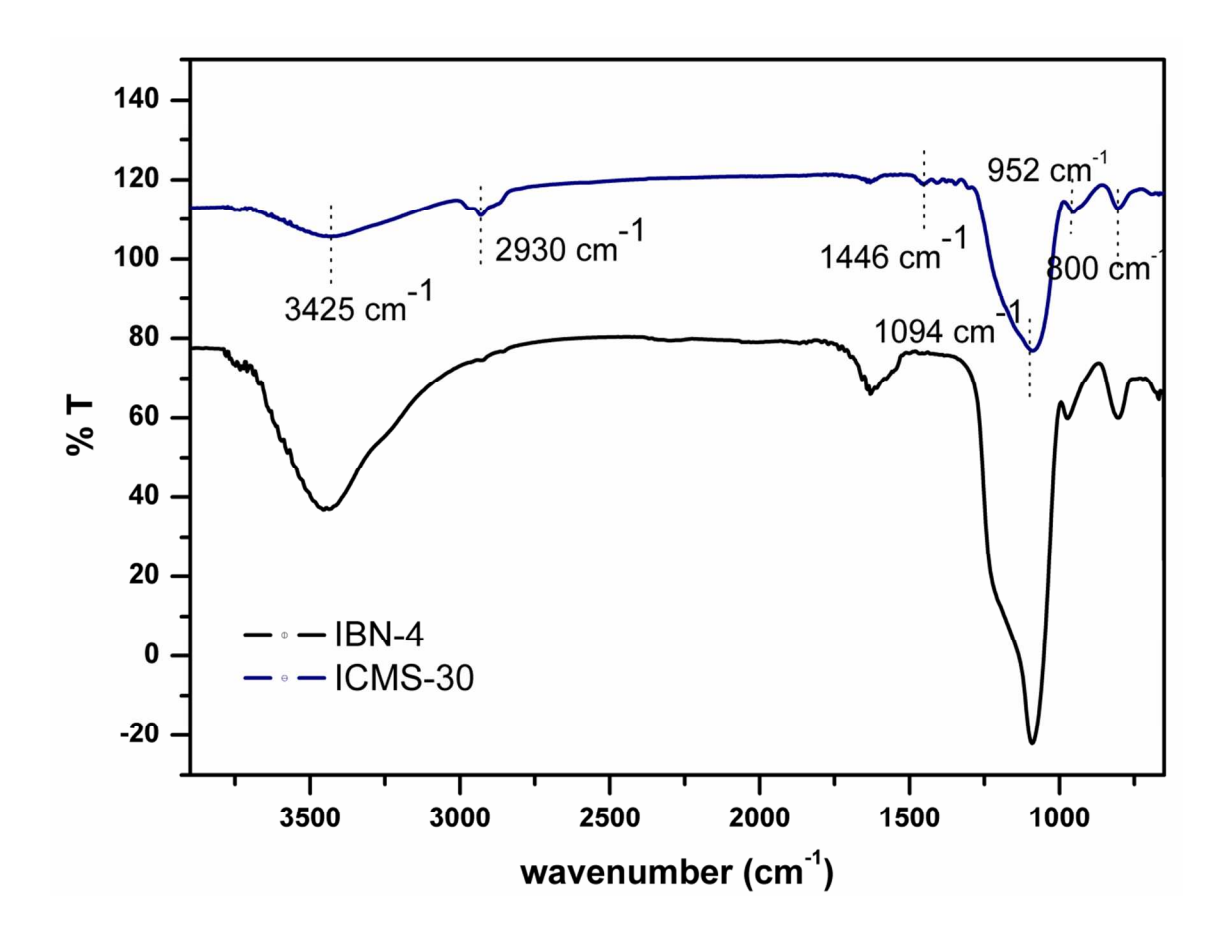


Figure 4. FT–IR spectra for IBN–4 and ICMS–30 materials.

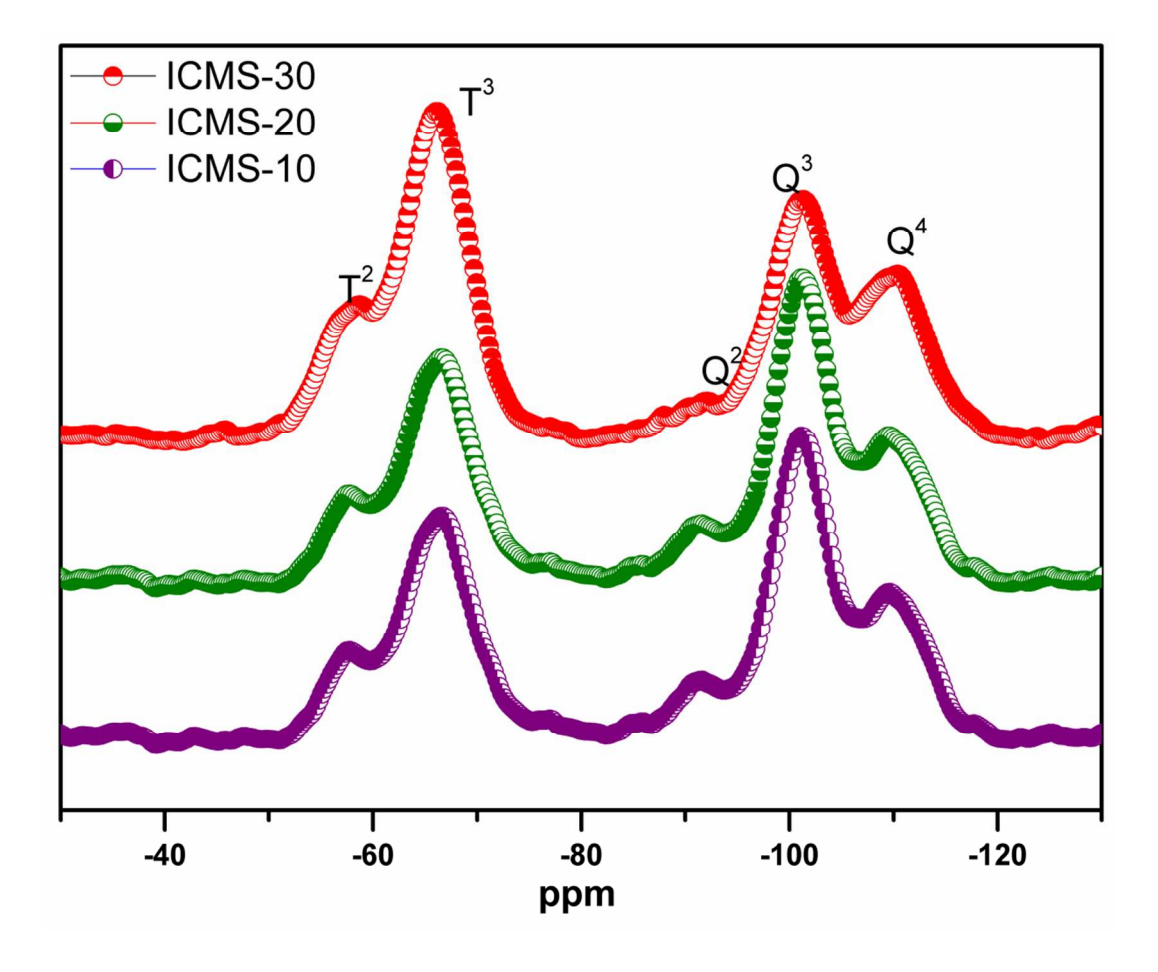


Figure 5. ²⁹Si CP/MAS NMR spectra for ICMS materials.

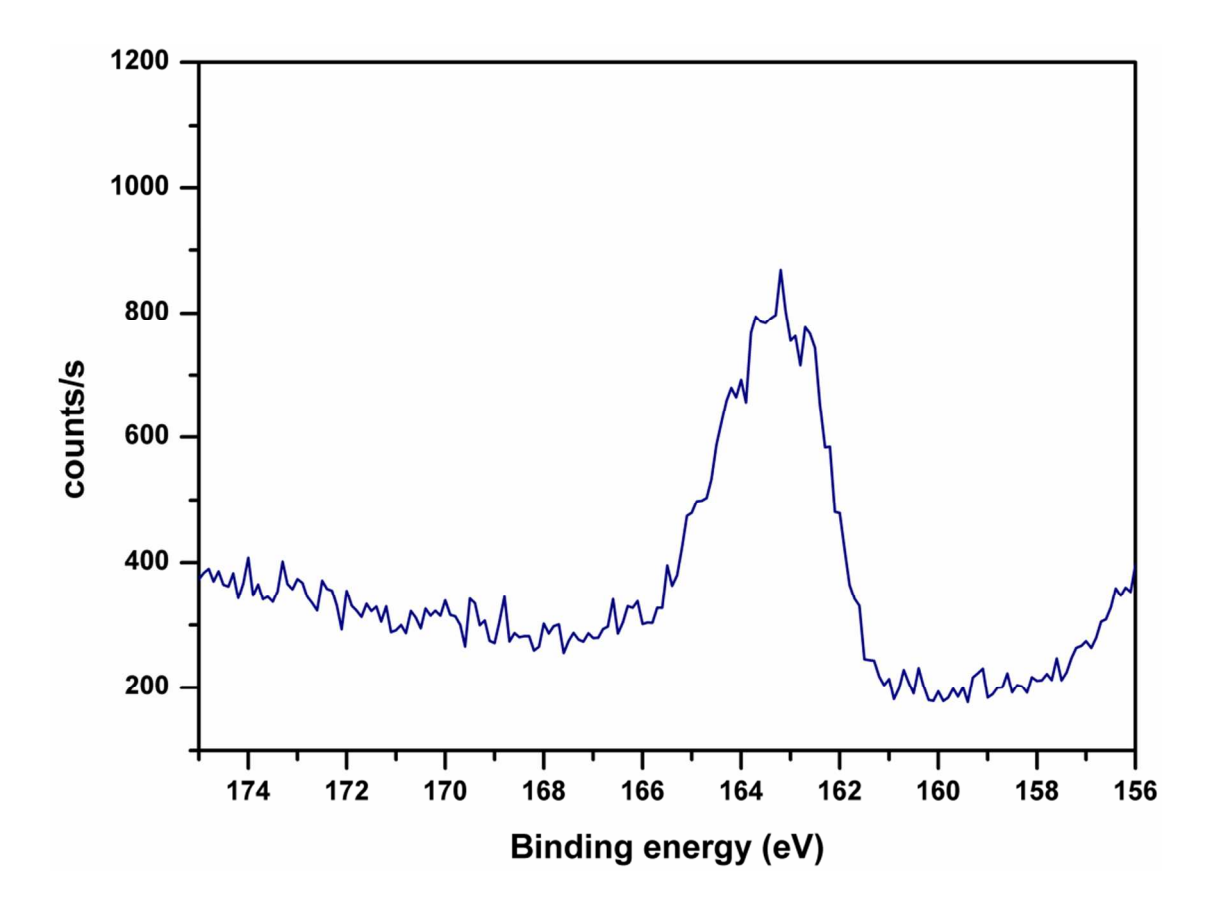


Figure 6: XPS pattern for S2p region of thiol groups in ICMS-30.

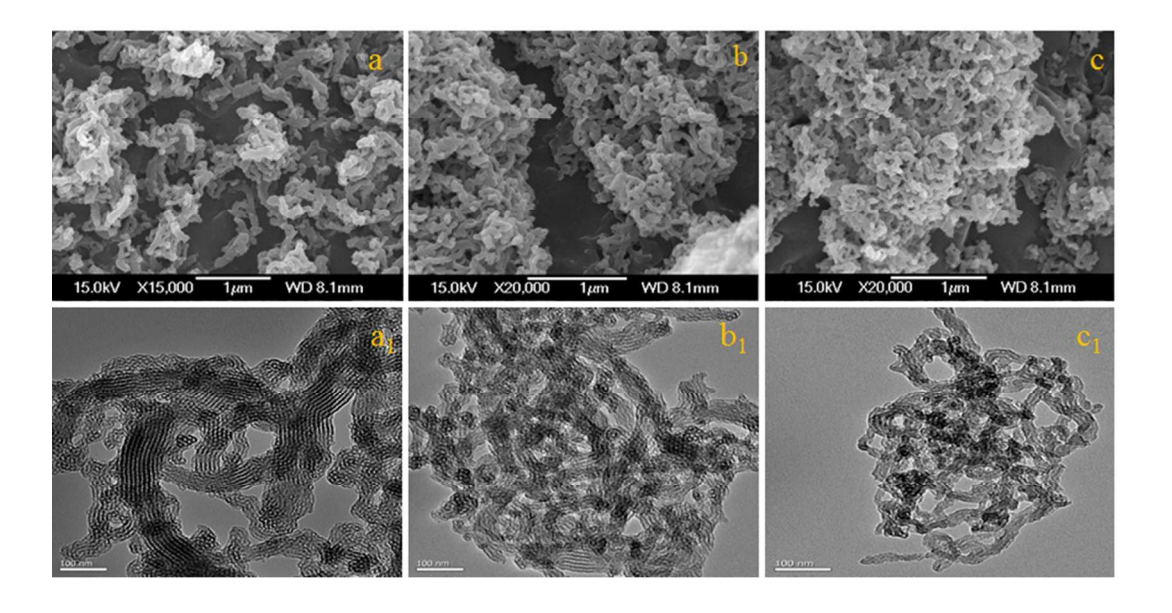


Figure 7. SEM images of ICMS materials; ICMS-10 (a), ICMS-20 (b), and ICMS-30 (c) and TEM images of ICMS materials; ICMS-10 (a₁), ICMS-20 (b₁), and ICMS-30 (c₁).

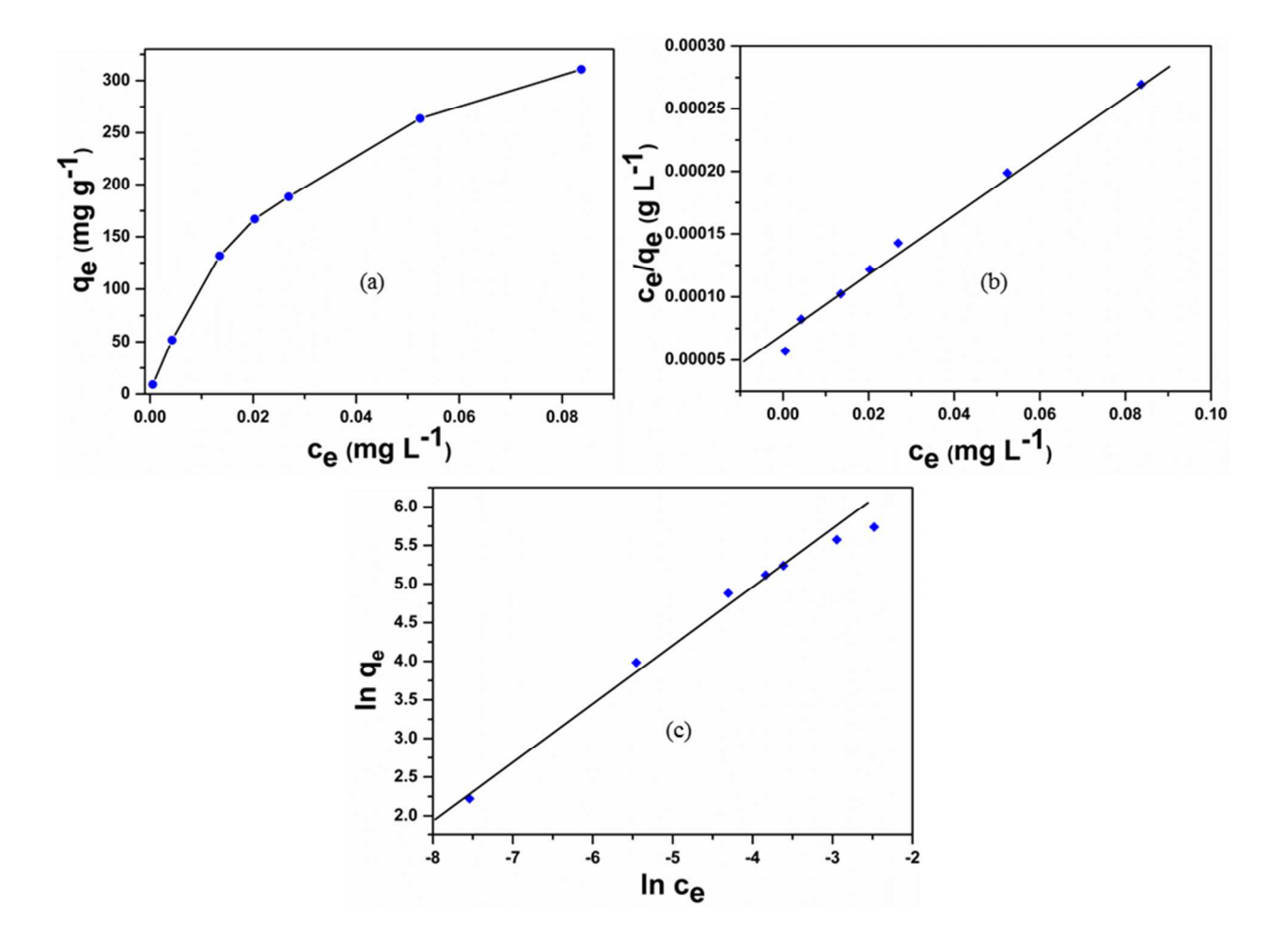


Figure 8. (a) Mercury adsorption isotherm of ICMS-30 at room temperature, (b) Langmuir adsorption isotherm, (c) Freundlich adsorption isotherm.

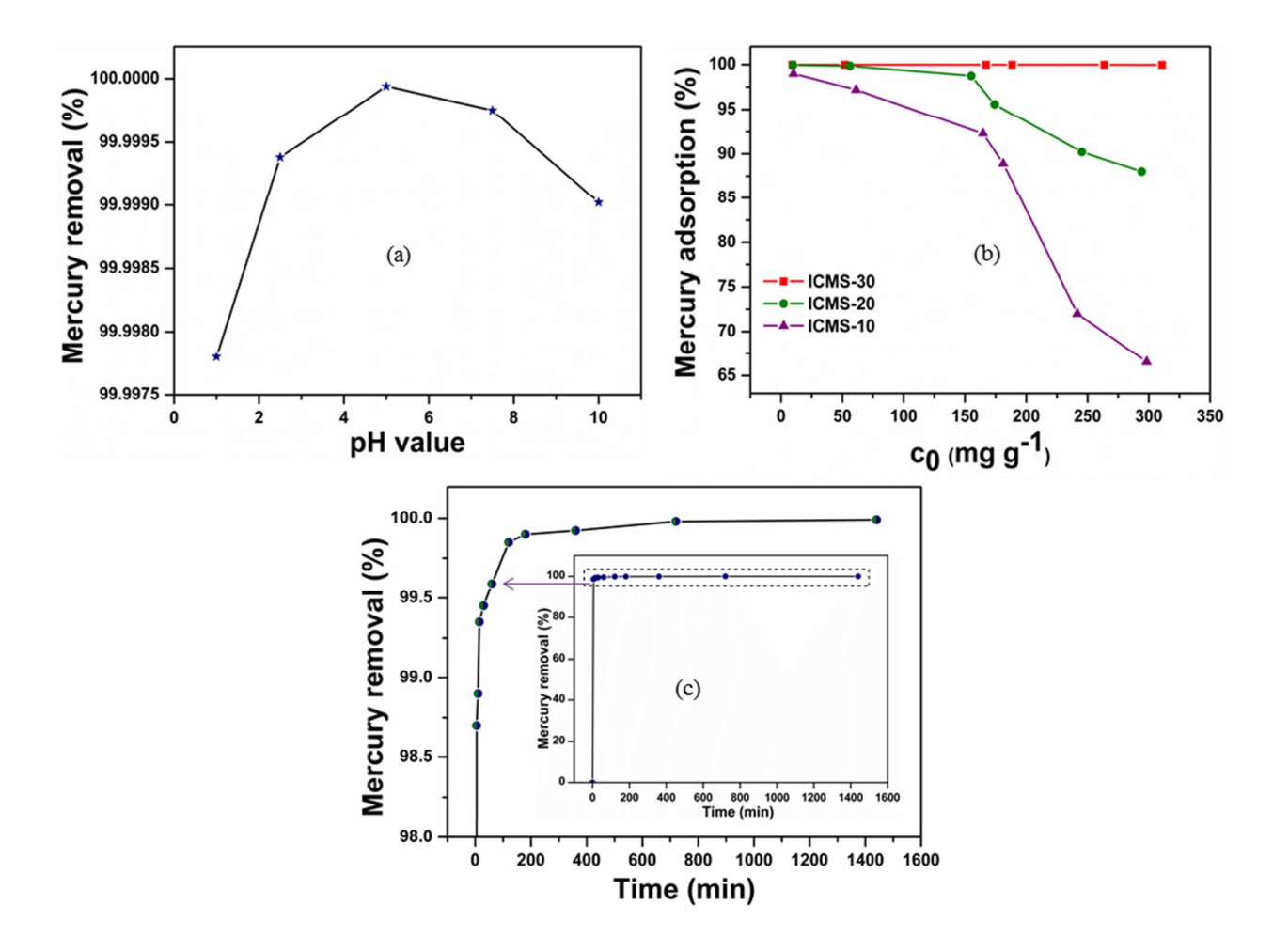


Figure 9. (a) Effect of pH on the binding affinity of mercury over ICMS-30, (b) Effect of initial mercury concentrations on the adsorption efficiency of ICMS materials, (c) Mercury removal efficiency of ICMS-30 with different time interval.

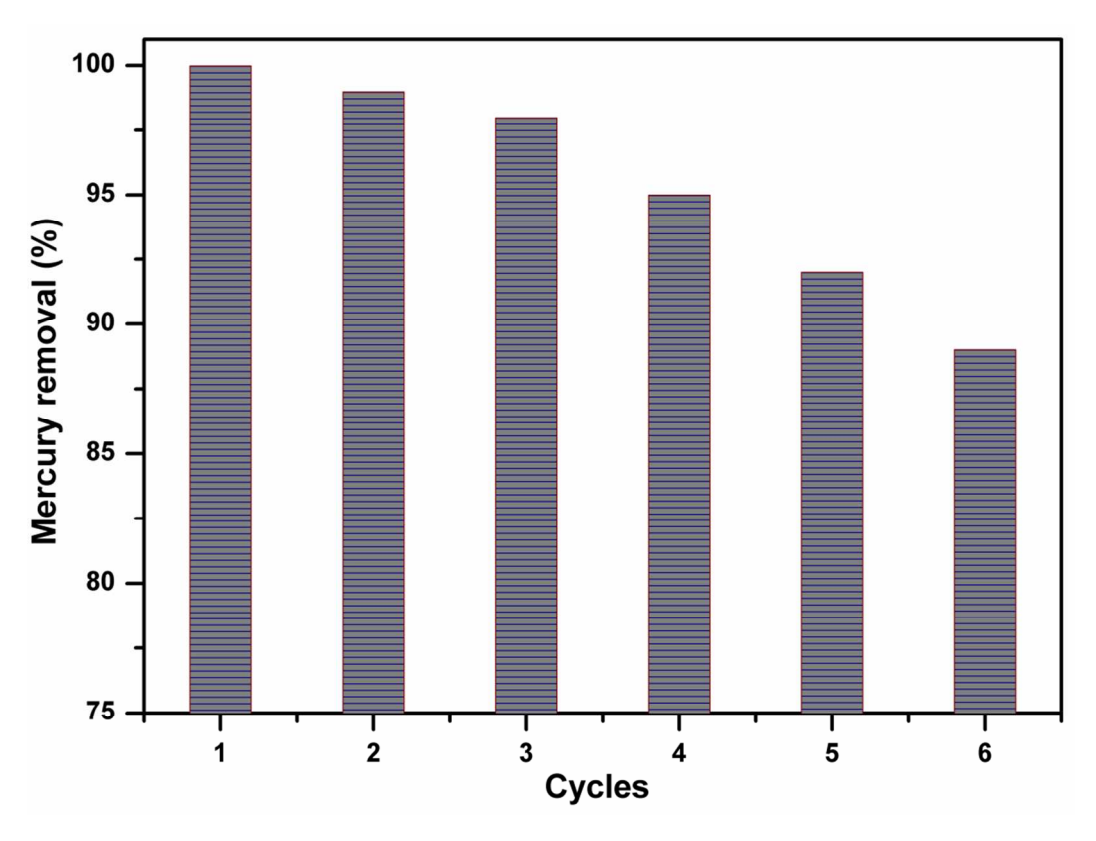


Figure 10. Adsorbent generation process (each cycle was applied 0.1g of Hg/1 g of ICMS-30).

Tables

Table 1. Physicochemical properties of IBN-4 and ICMS materials

Materials	d (nm)	S_{BET}^{a} (m^2/g)	D _p a (nm)	V_p^a (cm^3/g)	S ^b mmol/g
IBN-4	6.9	512	4.3	0.9	0
ICMS-10	7.5	486	4.2	0.40	1.27
ICMS-20	7.6	355	3.3	0.74	1.95
ICMS-30	8.0	302	3.2	0.45	2.87

Where d – spacing value, S_{BET} – surface area, D_p – pore diameter, V_p – pore volume, S – sulfur content (per gram of ICMS)

^a The results were obtained from N₂ sorption studies

^b The results were obtained from elemental analysis

Table 2. Adsorption isotherm

Langmuir adsorp	tion isotherm	Freundlich adsorption isotherm	
q _m (mg g ⁻¹)	b (L mg ⁻¹)	n	K
401	36.60	1.41	2271

 q_m – the maximum adsorption capacity of adsorbent, b – the affinity of binding sites or the Langmuir constant, K and n are constants represented indicative of adsorption capacity and intensity of adsorption respectively.

Table 3. Distribution coefficient (K_d) values of ICMS materials for mercury adsorption

Materials	K _d value
ICMS-10	2.515×10^5
ICMS-20	4.793×10^{6}
ICMS-30	1.739×10^7

Distribution coefficient (K_d) values were obtained from the experiments of 10 ppm Hg^{2+} solution.

Graphical abstract

Incessant formation of chain-like mesoporous silica with superior binding capacity for mercury

S. Ravi, M. Selvaraj*

New chain type mesoporous silica has been easily synthesized to remove the mercury ions from the aqueous medium.

